Hindawi
Geofluids
Volume 2021, Article ID 9968497, 13 pages
https://doi.org/10.1155/2021/9968497

Research Article

Status Quo of a CO_2-Assisted Steam-Flooding Pilot Test in China

Zongyao Qi,[1] Tong Liu,[1] Changfeng Xi,[1] Yunjun Zhang,[1] Dehuang Shen,[1] Hertaer Mu,[1] Hong Dong,[1] Aiping Zheng,[1] Kequan Yu,[1] Xiuluan Li,[1] Youwei Jiang,[1] Hongzhuang Wang,[1] Tayfun Babadagli,[2] and Huazhou Li[2]

[1]*State Key Laboratory of Enhanced Oil Recovery, PetroChina Research Institute of Exploration & Development, Research Institute of Petroleum Exploration & Development, PetroChina Co. Ltd, Beijing, China*
[2]*University of Alberta, Edmonton, Canada*

Correspondence should be addressed to Huazhou Li; huazhou@ualberta.ca

Received 20 March 2021; Revised 24 August 2021; Accepted 28 September 2021; Published 15 October 2021

Academic Editor: Ye Zhang

It is challenging to enhance heavy oil recovery in the late stages of steam flooding. This challenge is due to reduced residual oil saturation, high steam-oil ratio, and lower profitability. A field test of the CO_2-assisted steam flooding technique was carried out in the steam-flooded heavy oil reservoir in the J6 block of the Xinjiang oil field (China). In the field test, a positive response to the CO_2-assisted steam flooding treatment was observed, including a gradually increasing heavy oil production, an increase in the formation pressure, and a decrease in the water cut. The production wells in the test area mainly exhibited four types of production dynamics, and some of the production wells exhibited production dynamics that were completely different from those during steam flooding. After being flooded via CO_2-assisted steam flooding, these wells exhibited a gravity drainage pattern without steam channeling issues, and hence, they yielded stable oil production. In addition, emulsified oil and CO_2 foam were produced from the production well, which agreed well with the results of laboratory-scale tests. The reservoir-simulation-based prediction for the test reservoir shows that the CO_2-assisted steam flooding technique can reduce the steam-oil ratio from 12 m^3 (CWE)/t to 6 m^3 (CWE)/t and can yield a final recovery factor of 70%.

1. Introduction

Enhanced oil recovery (EOR) of heavy oil resources mainly focuses on the reduction of heavy oil viscosity [1]. Two methods are normally used: thermal methods and gas injection. Thermal methods are the most widely used techniques at present. Thermal methods rely on the use of heating to reduce the viscosity of heavy oil, leading to a larger recovery factor [2]. Gas injection (such as CO_2) is another important method of increasing recovery from light-oil reservoirs. Lab research and field practices have shown that CO_2 has a good solubility in light oil, which helps enhance the oil-swelling and viscosity reduction effect. CO_2 miscible flooding has achieved great success in light oil reservoirs [3–5]. Immiscible CO_2 injection (including CO_2 huff-and-puff and continuous CO_2 injection) is mainly explored for the cold recovery of heavy oil [1, 6–8]. CO_2 is rarely used in thermal recovery because the solubility of CO_2 is lower under high-temperature conditions, which negatively affects the viscosity reduction effect.

Steam flooding is used as a succession technique after steam huff-n-puff to effectively improve the recovery factor. Steam huff-n-puff is normally converted to steam flooding through conventional completion, in which multiple zones are perforated and produced in a commingled manner. However, such a direct conversion strategy has led to some problems, such as severe steam channeling, a high steam-oil ratio, a lower displacement efficiency, and poor economic benefits [9, 10]. In order to solve the problem of steam channeling, many oil fields have adopted a series of plugging control measures, including gas foam injection, high-temperature gel, and other profile control techniques [11–14]. Using these measures, the steam channeling direction can be changed in the short term, resulting in the short-term blocking of high-permeability channels, adjusting the steam absorption profile, expanding the steam-

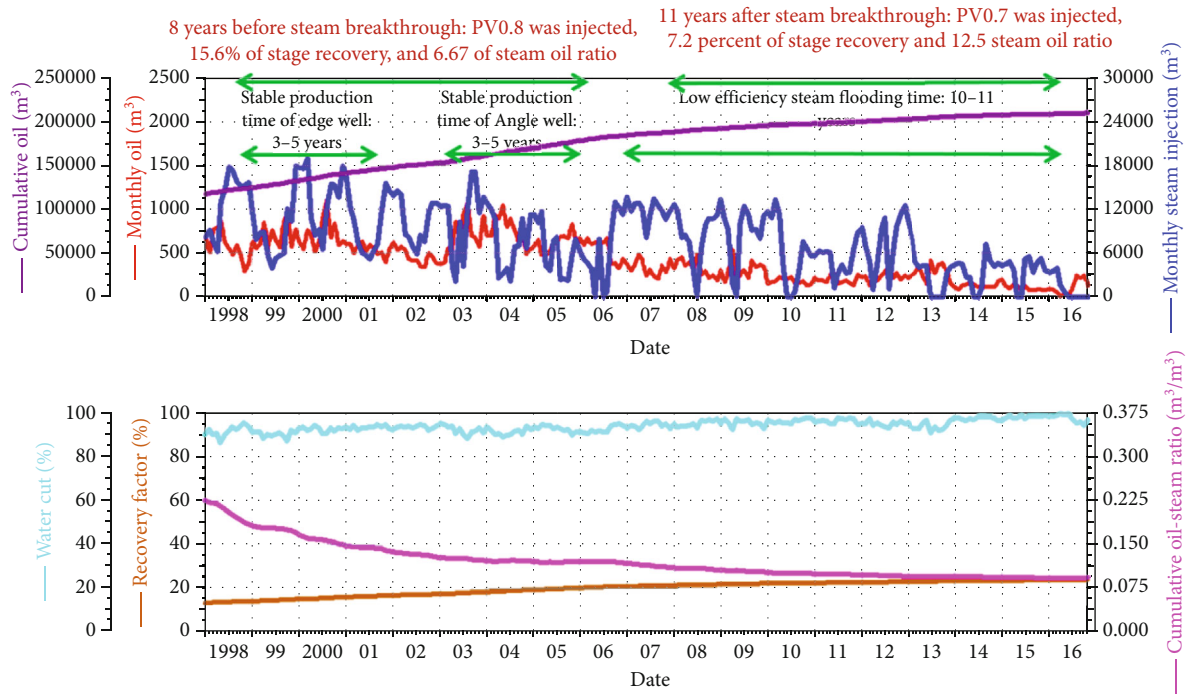

Figure 1: Production history of the test reservoir [7, 9].

sweeping volume to a certain extent, and thus improving the oil recovery factor. However, these profile control methods cannot help to improve the oil recovery in the long term since they cannot fundamentally solve the steam channeling problem or the other flooding problems. Therefore, it is highly important to develop and apply effective replacement techniques in the late stage of steam flooding. Both physical laboratory-scale experiments and numerical simulations have shown that by adjusting the perforation intervals and injecting CO_2 to assist the steam injection, the heavy oil recovery rate can be greatly improved, the steam-oil ratio can be reduced, and the performance of the later stage of steam flooding can be effectively improved. A field pilot test of CO_2-assisted steam flooding was conducted in the J6 block of the Xinjiang oil field. This paper reports the preliminary findings of this pilot test.

2. Geologic Background of the Test Area

The Xinjiang J6 block is a shallow heavy oil reservoir. The sedimentary environment is composed of a set of braided river delta front sediments, including estuary sand dams, tributary bays, and underwater distributary channel microfacies. The production layer system is $J_3q_2^{2-1} + J_3q_2^{2-2}$, which is composed of a set of fine to coarse grain sandstones. The $J_3q_2^{2-1}$ sand body has an average porosity of 30.3%, an average permeability of $2623 \times 10^{-3}\,\mu m^2$, and an average oil saturation of 78%. The thickness of the $J_3q_2^{2-1}$ layer is 13.0–25.0 m, with an average thickness of 18.0 m. The thickness of the $J_3q_2^{2-2}$ layer is 13.0–26.0 m, with an average thickness of 21 m. The $J_3q_2^{2-2}$ layer has an average porosity of 28.2%, an average permeability of $1200 \times 10^{-3}\,\mu m^2$, and an average oil saturation of 73%. These two layers have a high degree of heterogeneity. For instance, the permeability of the medium-fine sandstone at the top of the $J_3q_2^{2-1}$ and $J_3q_2^{2-2}$ layers ranges from 4000 mD to 5000 mD. A set of 0.5–2.0 m thick argillaceous sandstone, glutenite, and mudstone layers are sandwiched by the $J_3q_2^{2-1}$ and $J_3q_2^{2-2}$ layers. The permeability of the argillaceous sandstone and the glutenite layers varies from 100 mD to 800 mD. Nine well groups involving a total of 48 wells in the Xinjiang J6 block were selected to conduct the field test.

2.1. Development History of the Test Area. The test area was developed using an inverted nine-spot well pattern, with a total of 48 wells (i.e., nine steam injection wells and 39 production wells). Steam flooding began in 1998. In 2016, the steam-oil ratio reached 12 m^3 (CWE)/t, indicating that this reservoir could not be developed economically and faced possible shutdown. The overall development process can be divided into two stages: (1) the pre-steam-breakthrough stage and (2) the post-steam-breakthrough stage. Figure 1 shows the production history of the test reservoir. It can be seen from Figure 1 that in the eight years of production before steam breakthrough, a total of 0.8 PV was injected, the cumulative recovery was 15.6%, and the steam-oil ratio was 6.67 m^3 (CWE)/t. The oil recovery during the pre-steam-breakthrough stage was satisfactory, accompanied by a good heat utilization efficiency of the steam. A steam breakthrough event occurred after 2007. After the steam breakthrough, a total of 0.7 PV of steam was injected in 11 years, leading to an oil recovery of 7.2% and a steam-oil ratio of 12.5 m^3 (CWE)/t. It is obvious that, in the post-steam-breakthrough stage, the heat utilization efficiency of the steam steeply declined, leading to a reduced oil recovery efficiency. After the steam breakthrough, the production wells

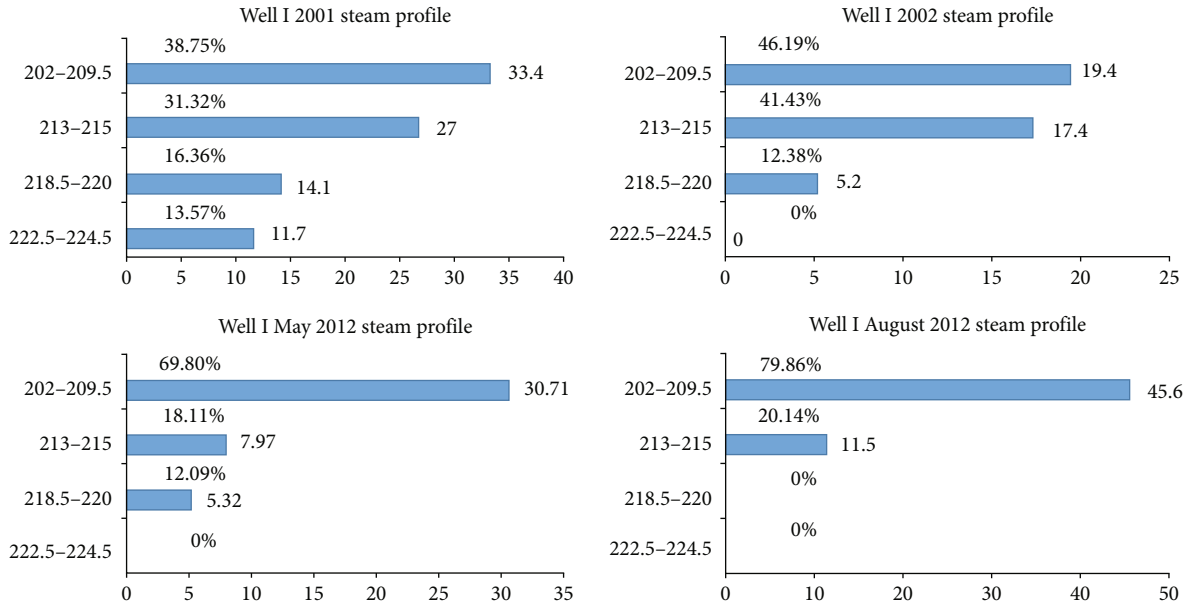

Figure 2: Variation in the steam absorption profiles of well I in the Xinjiang J6 block [7, 9].

exhibited high-temperature and high-water-cut characteristics. In addition, the steam was mainly concentrated in the 2–3 m thick oil layer at the top of $J_3q_2^{2\text{-}1}$, leading to preferential flooding and ineffective steam circulation. The volume of the steam chamber was difficult to expand further. Intermittent steam injection and intermittent opening of the oil wells for production were implemented to maintain production in an inefficient way [15]. Figure 2 shows the variation in the steam absorption profiles of well I in the Xinjiang J6 block. It can be seen from Figure 2 that after steam breakthrough, there was a steam adsorption peak in the top part of the perforation interval.

2.2. Remaining Oil Distribution. In order to clarify the distribution characteristics of the remaining oil in the test area and to provide a basis for adjusting the well pattern and perforation intervals, four wells were drilled in the test area and were subsequently cored to study the distribution of the remaining oil. Figure 3 shows a schematic diagram showing the locations of the nine test wells (solid blue circles) and the three cored wells (solid red circles).

According to the statistics of the cored wells, the distribution characteristics of the remaining oil in the J6 block can be summarized as follows: (1) the oil saturation of the $J_3q_2^{2\text{-}1}$ layer gradually increased from top to bottom, and the same was true for the $J_3q_2^{2\text{-}2}$ layer; (2) the $J_3q_2^{2\text{-}1}$ and $J_3q_2^{2\text{-}2}$ layers had low remaining oil saturation in their upper parts because preferential steam flooding occurred in these locations; (3) the challenging steam issues at the top of the $J_3q_2^{2\text{-}1}$ layer were more serious than those at the top of the $J_3q_2^{2\text{-}2}$ layer; and (4) layers $J_3q_2^{2\text{-}1}$ and $J_3q_2^{2\text{-}2}$ were two relatively independent flow units. The interlayers served as an effective impermeable barrier between $J_3q_2^{2\text{-}1}$ and $J_3q_2^{2\text{-}2}$, resulting in the injected steam failing to pass through the interlayers and staying within the two production layers.

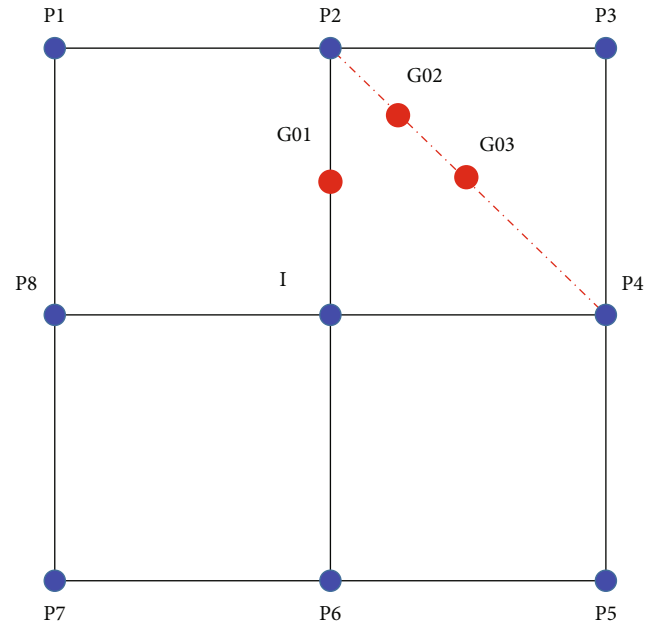

Figure 3: Schematic diagram showing the locations of the nine test wells (solid blue circles) and the three cored wells (solid red circles) [7, 9].

Table 1 presents a statistical summary based on the information obtained from the cored wells. On average, the initial oil saturation of the $J_3q_2^{2\text{-}1}$ layer was higher than that of the $J_3q_2^{2\text{-}2}$ layer. Although the overall recovery factor of the $J_3q_2^{2\text{-}1}$ layer was 10–15% higher than that of layer $J_3q_2^{2\text{-}2}$, there was still a great recovery potential in the middle and lower parts of the $J_3q_2^{2\text{-}1}$ layer.

Based on the coring results obtained after steam flooding, $J_3q_2^{2\text{-}1}$ and $J_3q_2^{2\text{-}2}$ represented two relatively independent flow units, both of which formed steam channels, resulting in low remaining oil saturations at the tops of the

Table 1: Statistical summary based on the information obtained from the cored wells [7, 9].

Oil layer	Initial oil saturation of adjacent well (%)			Oil saturation of cores (%)	Recovery factor (%)
	Well G01 compared to its adjacent wells				
	Adjacent well P7	Adjacent well P8	Average	G01	
$J_3q_2^{2\text{-}1}$	76.5	78.7	77.6	55.7	28.22
$J_3q_2^{2\text{-}2}$	72.1	70.8	71.5	57.7	19.24
	Well G02 compared to its adjacent wells				
Oil layer	Initial oil saturation of adjacent wells (%)			Oil saturation of cores (%)	Recovery factor (%)
	Adjacent well P7	Adjacent well P8	Average	G02	
$J_3q_2^{2\text{-}1}$	76.5	78.7	77.6	29.9	61.47
$J_3q_2^{2\text{-}2}$	72.1	70.8	71.5	40.5	43.32
	Well G03 compared to its adjacent wells				
Oil layer	Initial oil saturation of adjacent wells (%)			Oil saturation of cores (%)	Recovery factor (%)
	Adjacent well P7	Adjacent well I	Average	G03	
$J_3q_2^{2\text{-}1}$	76.5	76.1	76.3	40.6	46.79
$J_3q_2^{2\text{-}2}$	72.1	62.8	67.5	41.9	37.88
	Total contrast between adjacent wells and cored wells				
Oil layer	Initial oil saturation of adjacent wells (%)			Oil saturation of cores (%)	Recovery factor (%)
			Average	Average	
$J_3q_2^{2\text{-}1}$			77.2	42.1	45.49
$J_3q_2^{2\text{-}2}$			70.1	46.7	33.40

two oil layers. Both layers exhibited increasing oil saturation from top to bottom, which was partially due to the vertical heterogeneity of the permeabilities of the two layers. In view of the above phenomenon and the actual properties of the reservoir, a numerical simulation model was established (Figure 4). The model simulates an inverse nine-point well pattern. There are nine wells in the model, with a steam injection well in the middle and production wells around it. The grid size of the model is 140 m × 140 m × 29 m, and the grid resolution is 9.3 m × 9.9 m × 1 m, with a total of 6525 grids. The net gross ratio of the model is 0.55, the average porosity of reservoir $J_3q_2^{2\text{-}1}$ is 0.3, the porosity of reservoir $J_3q_2^{2\text{-}2}$ is 0.28, and the porosity of the interlayer is 0.05. The permeability of $J_3q_2^{2\text{-}1}$ varied from 5000 mD to 1200 mD from top to bottom, with an average value of 2600 mD. The permeability of $J_3q_2^{2\text{-}2}$ varied from 4500 mD to 800 mD from top to bottom, with an average value of 1100 mD. There was a 1 m thick physical interlayer between the $J_3q_2^{2\text{-}1}$ and $J_3q_2^{2\text{-}2}$ layers. The two sets of numerical simulation results were compared. From the model, it was found that there were high permeability layers on the tops of $J_3q_2^{2\text{-}1}$ and $J_3q_2^{2\text{-}2}$. The purpose of the model was to simulate whether the interlayer permeabilities of 50–400 mD had an impact on the residual oil distribution law of each reservoir when the bottom hole steam quality was 0.6 and 0.3, representing high-quality and low-quality steam, respectively. Both the production wells and the steam injection wells adopted a perforation method which perforates the entire reservoir section.

Figure 5 shows the simulation results for a steam quality of 0.6. When the steam quality was 0.6 and the permeability of the interlayer was greater than 100 mD, the low oil saturation zone located at the top of $J_3q_2^{2\text{-}2}$ did not appear. When the permeability of the interlayer was less than 100 mD, the low oil saturation zone located at the top of $J_3q_2^{2\text{-}2}$ started to appear. This means that the interlayer permeability may play an important role in the sweeping efficiency in the lower $J_3q_2^{2\text{-}2}$ layer. When the quality was 0.6, the fluid entering the high-permeability layer at the top of the $J_3q_2^{2\text{-}2}$ layer was mainly steam. So, when the permeability of the interlayer was greater than 100 mD, the interlayer did not have the ability to block the steam's permeation, allowing it to permeate through the interlayer and into the upper oil layer. The low oil saturation zone at the top of $J_3q_2^{2\text{-}2}$ was not obvious.

Figure 6 shows the simulation results for a steam quality of 0.3. When the steam quality was 0.3, even when the interlayer permeability increased from 50 to 800, there were low oil saturation areas at the top of layer $J_3q_2^{2\text{-}1}$ and layer $J_3q_2^{2\text{-}2}$ for all of the calculation results. The reason for this phenomenon is that the liquid phase is the main component in low dryness steam. Due to the gravity differentiation, layer $J_3q_2^{2\text{-}2}$ was mainly hot water driven, and layer $J_3q_2^{2\text{-}1}$ was mainly steam driven. At this time, the injection medium had a great impact on the distribution of the remaining oil.

It can be seen from the calculation results that both the injected medium and the interlayer affect the distribution pattern of the remaining oil. The interlayer between $J_3q_2^{2\text{-}1}$ and $J_3q_2^{2\text{-}2}$ in the J6 block is mainly argillaceous sandstone with a permeability of 200–800 mD, which does not have the ability to block steam flow. Under the condition of high-quality steam injection, the steam can effectively penetrate the interlayer and form effective steam-oil gravity segregation over the two layers. Therefore, the low dryness of the injected steam is the reason for the formation of this residual oil distribution pattern. In the later stage of steam

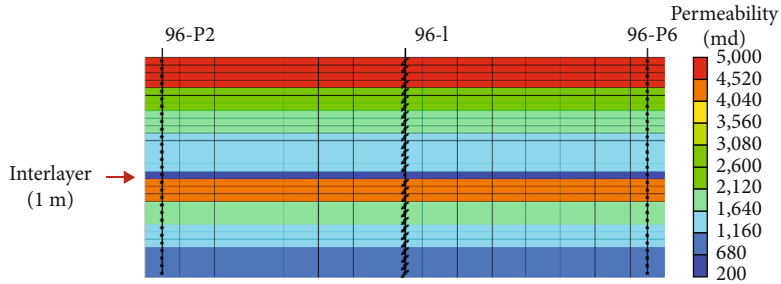

Figure 4: Numerical simulation model built to simulate the steam flooding process in the $J_3q_2^{2\text{-}1}$ and $J_3q_2^{2\text{-}2}$ layers.

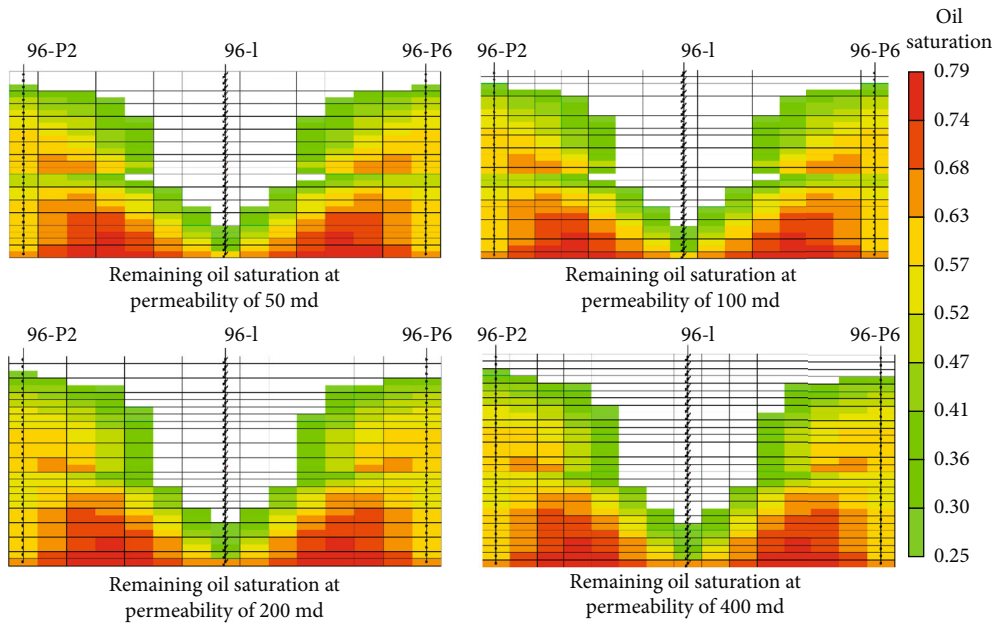

Figure 5: Remaining oil saturation profiles simulated under different interlayer permeabilities after steam flooding for 2600 days. A constant steam quality of 0.6 was used in these simulations.

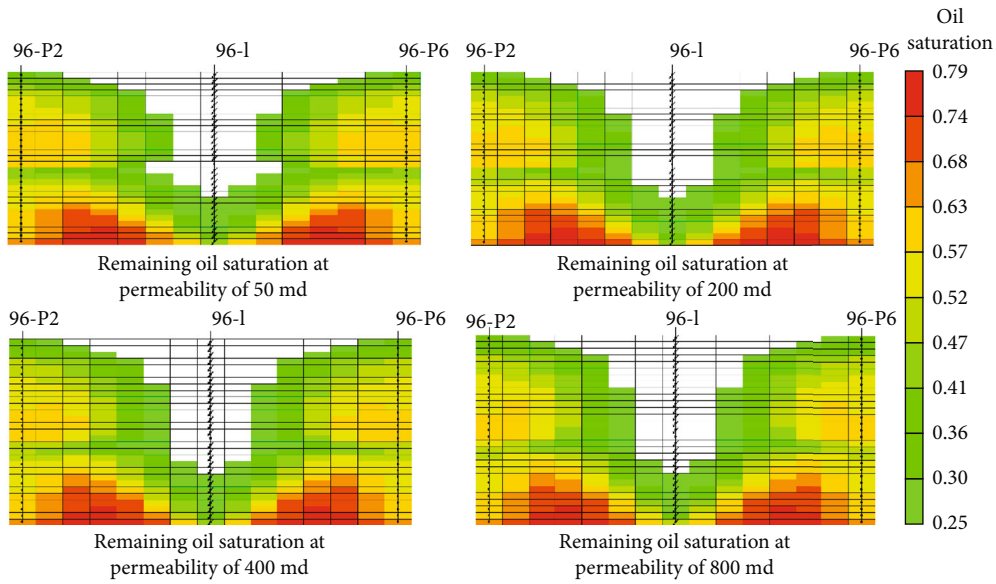

Figure 6: Remaining oil saturation profiles simulated under different interlayer permeabilities after steam flooding for 5400 days. A constant steam quality of 0.3 was used in these simulations.

flooding, intermittent steam flooding and low-quality hot water flooding are normally used to mitigate the steam channeling issue. Then, the remaining oil distribution will be dominated by the hot water flooding process (Figure 6). In this hot-water-flooding-dominated case, the channeling issue in both layers becomes more severe than that in the steam-flooding-dominated process.

2.3. Engineering Design of CO_2-Assisted Steam Flooding

2.3.1. Perforation Design. Nine well groups in the later stage of steam flooding in the J6 block were selected as pilot test areas for the CO_2-assisted steam flooding technique. The test area was basically in a state of shutdown before the conversion. The total daily oil production of the nine well groups was 10 t, the steam-oil ratio was 12.5, and the recovery factor was 45%. Because traditional steam flooding adopts a perforation scheme in which both zones are fully perforated, once the steam breaks through to the production well more steam will be produced, resulting in an invalid steam circulation.

The above discussion shows that the interlayers between $J_3q_2^{2\text{-}1}$ and $J_3q_2^{2\text{-}2}$ are mainly argillaceous sandstones. Since the interlayers cannot block the steam flow, they can be developed as a single layer. The adjustment of the perforation scheme is shown in Figure 7. As shown by Figure 7, partial perforation was implemented in the middle and lower parts of the $J_3q_2^{2\text{-}2}$ layer to prevent the steam from breaking through to the production well from the upper high-permeability zones of the two layers. By coinjecting CO_2 and high-quality steam into the middle and lower part of the $J_3q_2^{2\text{-}2}$ layer, the steam could rise and pass through the interlayer, which effectively produced the heavy oil in the middle and lower parts of the $J_3q_2^{2\text{-}1}$ layer and the heavy oil in the upper part of the $J_3q_2^{2\text{-}2}$ layer. Subcool control can also be leveraged to achieve a gravity drainage production model, which helps to fundamentally solve the problem of steam channeling.

Table 2 and Figure 8 show the simulation results and the effect of perforation thickness on the production performance. The smaller the perforation thickness, the closer the perforation position to the bottom of $J_3q_2^{2\text{-}2}$. This will help create a longer effective production time and will ultimately lead to a higher cumulative oil production. Overall, in the numerical simulation model, the smaller the perforation thickness, the lower the initial liquid production, but the perforation thickness has little effect on the liquid production. Due to the heterogeneity of the actual reservoir, in order to ensure that the production well can produce liquid normally and has more upper space for gravity oil drainage, it is recommended that the perforation thickness be 4–5 m.

2.3.2. Injection Volume Design. Numerical simulations were conducted to examine the effect of coinjecting different amounts of CO_2 and steam on the production performance. Based on the simulation results, we found that the reservoir responds to the coinjection of CO_2 and steam in a more favorable way than to pure steam injection. The peak oil production was also found to be higher. Figure 9 shows the effect of coinjecting different amounts of CO_2 with 50 t of steam on the production performance. As can be seen from Figure 9, adding more CO_2 to the steam results in a faster production response and a higher peak oil production. Further careful checking of the additional cumulative oil produced per ton of CO_2 injected indicates that injecting 1 ton of CO_2 with 50 t of steam provides the optimal performance, leading to an additional 2–3 m^3 of oil production per ton of CO_2 injected.

From an operational point of view, an alternating injection mode can be more easily implemented than a coinjection mode. After careful consideration, the field test was conducted by alternatively injecting a larger slug of steam and a much smaller slug of CO_2. In the field test, the CO_2 was injected in the form of a small slug, and each slug contained 10 tons of CO_2. The steam injection was stopped when the CO_2 was injected, and the steam injection was resumed after the CO_2 injection was completed. Each injection cycle lasted around 10 days. This injection strategy could help mitigate the corrosion problem caused by CO_2 injection, but the injection pressure should be strictly monitored to ensure that the fluctuation in the injection pressure does not exceed 20% of the designed pressure value. This was done to avoid the scenario in which the subcooling in the production well becomes difficult to control due to excessive pressure fluctuations.

3. Preliminary Results of the Field Test

3.1. Production Response of the Test Area to CO_2-steam Coinjection. The CO_2-steam coinjection was started at the end of October 2018. Figure 10 shows the production profiles of the test area in response to the CO_2-steam coinjection. After CO_2-steam coinjection, the fluid production in the early stage of the field test increased steadily, while its oil cut also exhibited an increasing trend. Both the steam-oil ratio and the water cut showed an effective reduction. Figure 11 shows the average wellhead pressure and the production-injection ratio recorded during the field test. The instantaneous production-injection ratio in the test area remained larger than 1.5 after November 2018. The average oil (wellhead) pressure increased from the initial value of 0.01 MPa to 0.15 MPa, indicating that the formation was reenergized by the CO_2 injection. Overall, the reservoir responded fairly well to the CO_2-steam coinjection.

Figure 10 further shows that the liquid production could not be effectively curbed, exhibiting a continuously increasing trend. It should be noted that there are active water bodies in the eastern and southern parts of the test area. The water recovery rate (i.e., the ratio of the produced water to the injected water) in the steam huff-n-puff+steam flooding stage was 136%, indicating that the test area was already under the influence of water invasion from the water bodies. As of January 31, 2020, the water recovery rate during the CO_2-assisted steam flooding stage had reached 114.67%, which was lower than the recovery rate experienced in the steam huff-n-puff+steam flooding stage, so the injection of CO_2 can control the water invasion. Unfortunately, since January 2020, due to the impact of COVID-19, the on-site injection of CO_2 was stopped. Although the production-

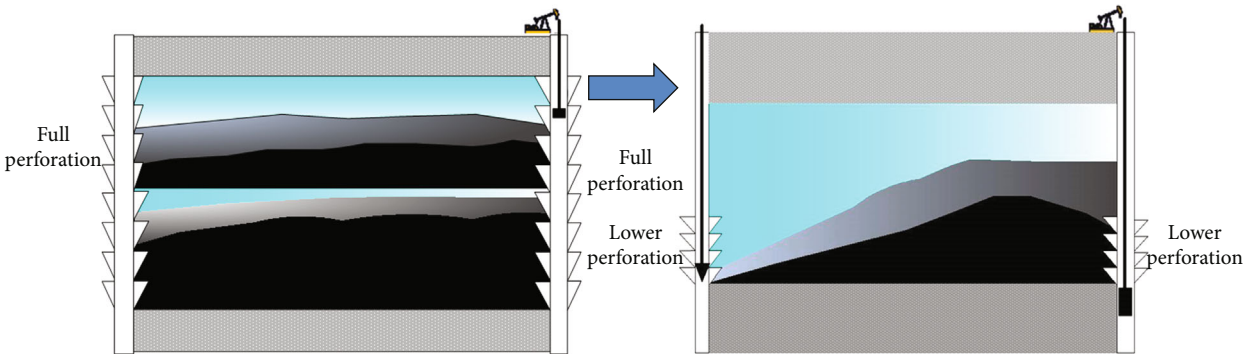

Figure 7: Adjustment of the perforation scheme.

Table 2: Simulated reservoir production performance under different perforation thicknesses.

Scheme	Effective production time (day)	Cumulative oil production (t)	Cumulative steam injection (m^3)	Cumulative steam-oil ratio (m^3 (CWE)/t)
Perforation 7.2 m	1364	11919.83	68250	0.175
Perforation 5.8 m	1485	12468.15	74250	0.168
Perforation 4.5 m	1706	13470	85500	0.158
Perforation 3.6 m	2023	14162.55	101250	0.140
Perforation 2.7 m	2555	15270.45	127750	0.120

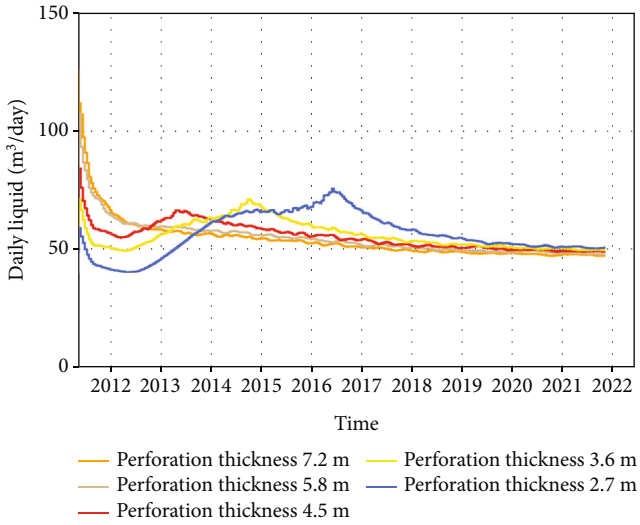

Figure 8: Daily liquid production simulated under different reservoir thicknesses.

injection ratio was still higher than 1.5 (Figure 11), the water cut increased to about 96% and the average wellhead pressure decreased from 0.15 MPa to 0.062 MPa. After stopping the CO_2 injection, the production to injection ratio increased, which led to a decrease in the formation pressure. This decrease in pressure could further aggravate the water invasion issue, leading to an increase in the water cut and a decrease in the oil production. At present, the test area is undergoing operational adjustment.

3.2. Classification of Production Wells in the Test Area. Based on the analysis of the production dynamics in the early stage of the CO_2-steam coinjection, it was found that the production wells in the test area exhibited four different types of dynamic production characteristics.

The first type (type I well) was characterized by a high produced-liquid temperature and a large liquid production after conversion. Figure 12 shows the production dynamics of this type of well. After only opening the perforation interval in the lower part of the $J_3q_2^{2\text{-}2}$ layer, this type of well was converted to CO_2-assisted steam flooding. The produced-liquid temperature increased in the beginning of the production stage, generally at a temperature of ~100°C. In addition, a larger liquid production volume ensued. Such wells were deemed to have sufficient residual energy in the middle and lower parts of the $J_3q_2^{2\text{-}2}$ layer during the previous steam flooding stage. Moreover, this type of well has a very good connection with the steam injection well, so it had a high temperature and a high liquid volume at the beginning of conversion and such pattern remained stable for a long time. As such, strict liquid withdrawal control measures needed to be implemented in these wells to prevent steam/gas channeling.

The type II wells exhibited a gradual decrease in both the fluid production volume and the produced-liquid

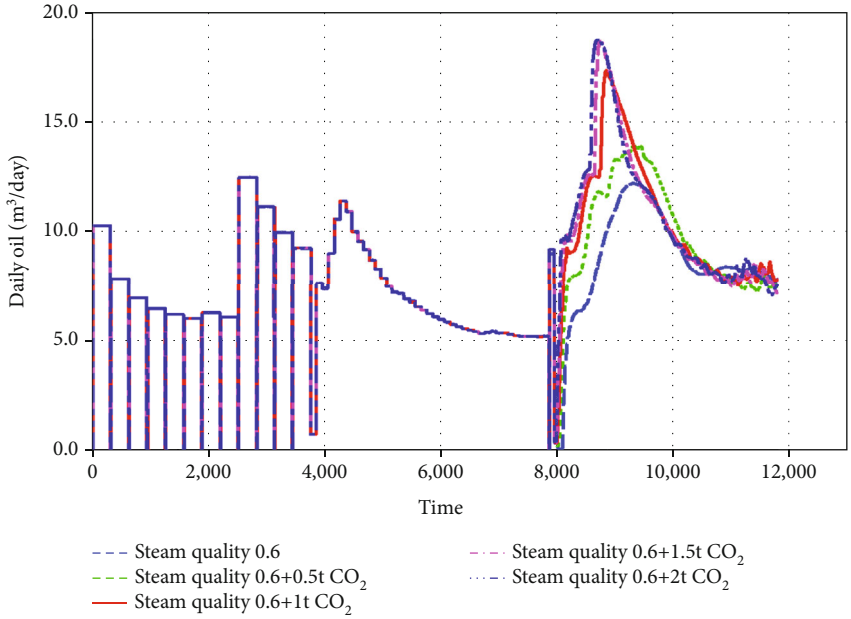

Figure 9: Effect of coinjecting different amounts of CO_2 with 50 t of steam on the production performance.

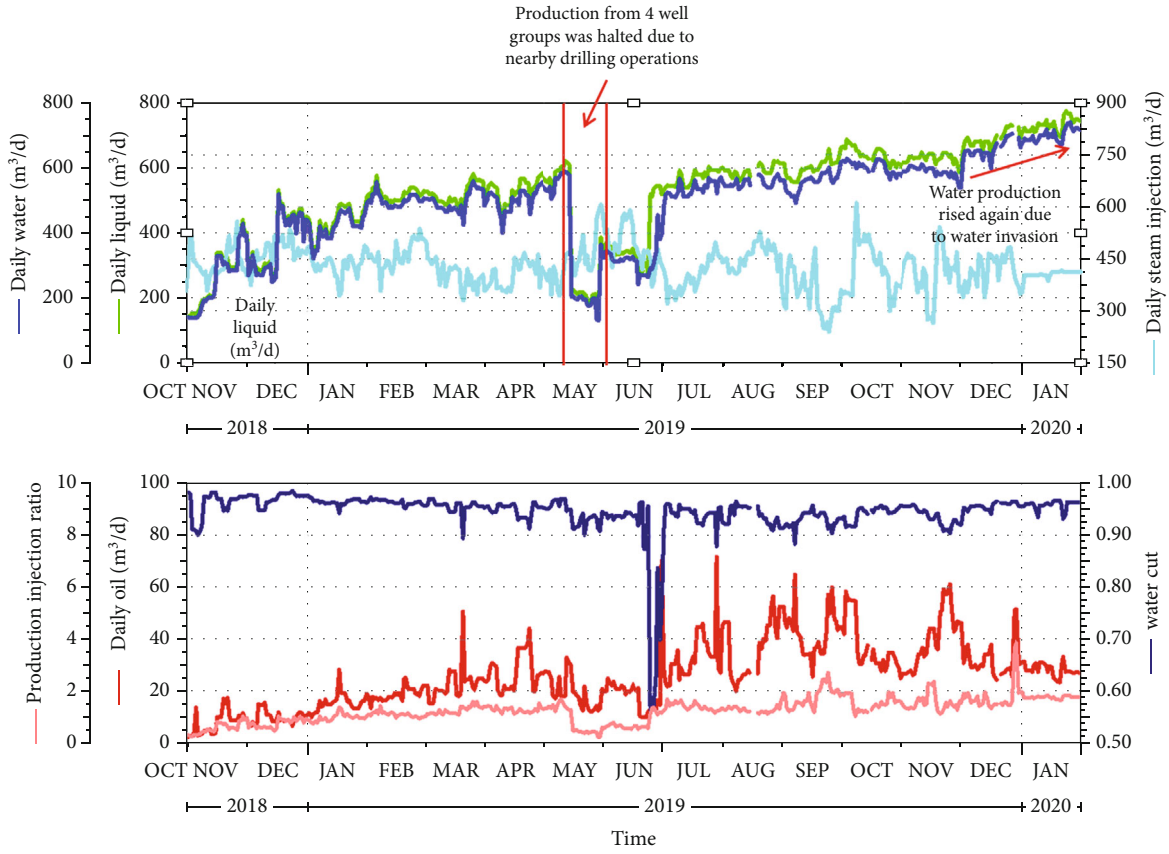

Figure 10: Production profiles of the test area in response to CO_2-steam coinjection.

temperature after conversion. Figure 13 shows the production dynamics of this type of well. These wells were able to recover certain areas of the middle and lower parts of $J_3q_2^{2\text{-}2}$. At the beginning, the $J_3q_2^{2\text{-}2}$ layer in these wells also had a large amount of residual energy from the original steam flooding, just like the type I wells, but the difference

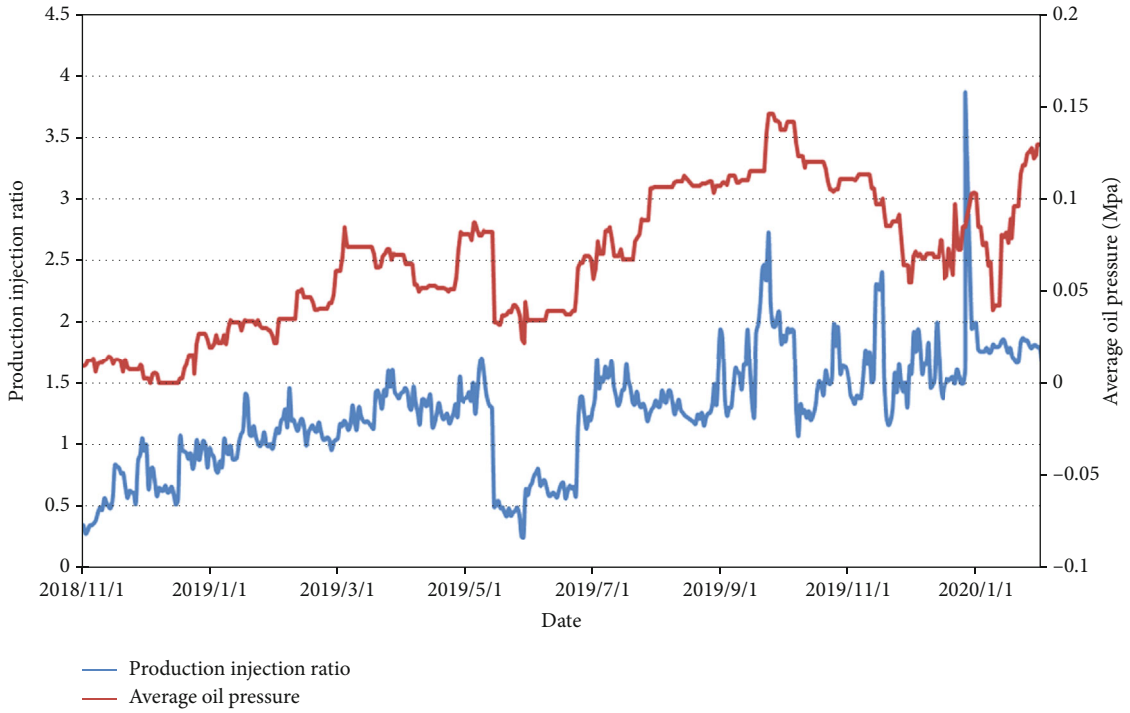

Figure 11: Average wellhead pressure and production injection ratio in the test area recorded during the field test.

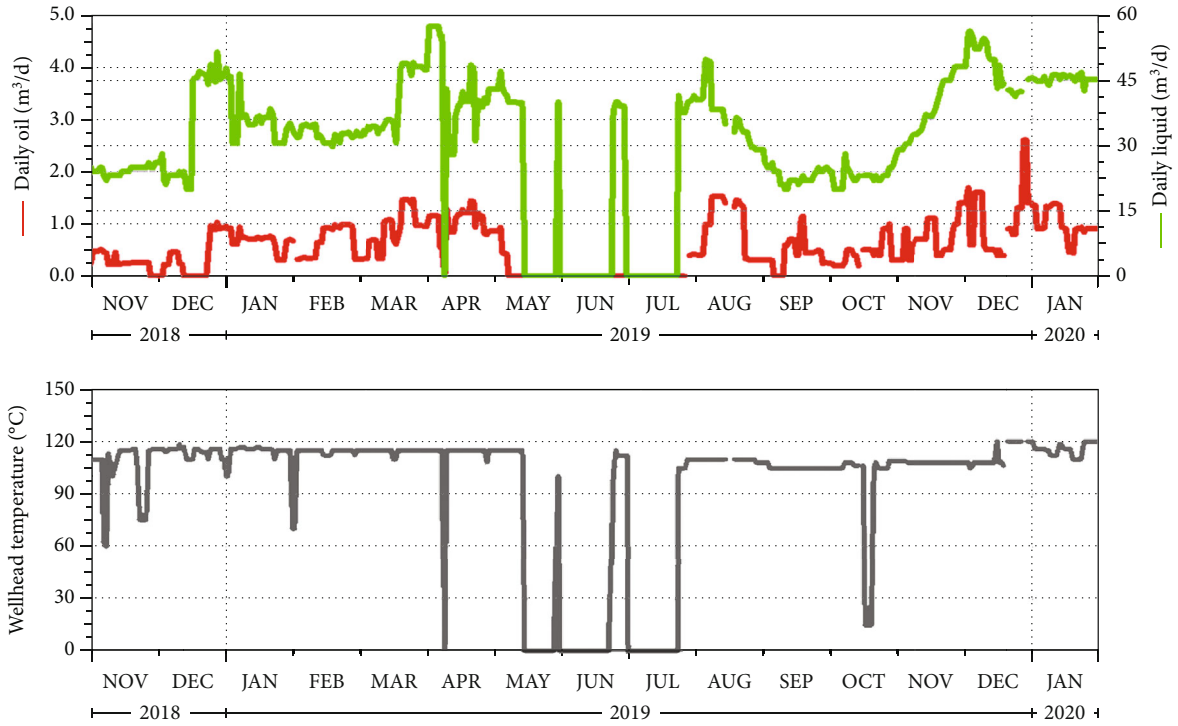

Figure 12: Typical production curves for a type I well.

was that these producers did not have a stable connection with the steam injection well, and the energy supplemented by the CO_2-steam coinjection was insufficient. Therefore, when all of the remaining energy was produced, the energy supply was insufficient, so the liquid production and liquid temperature decreased. Some of these types of wells could be developed after a period of time, resulting in a gradual increase in fluid production. If no fluid was produced in

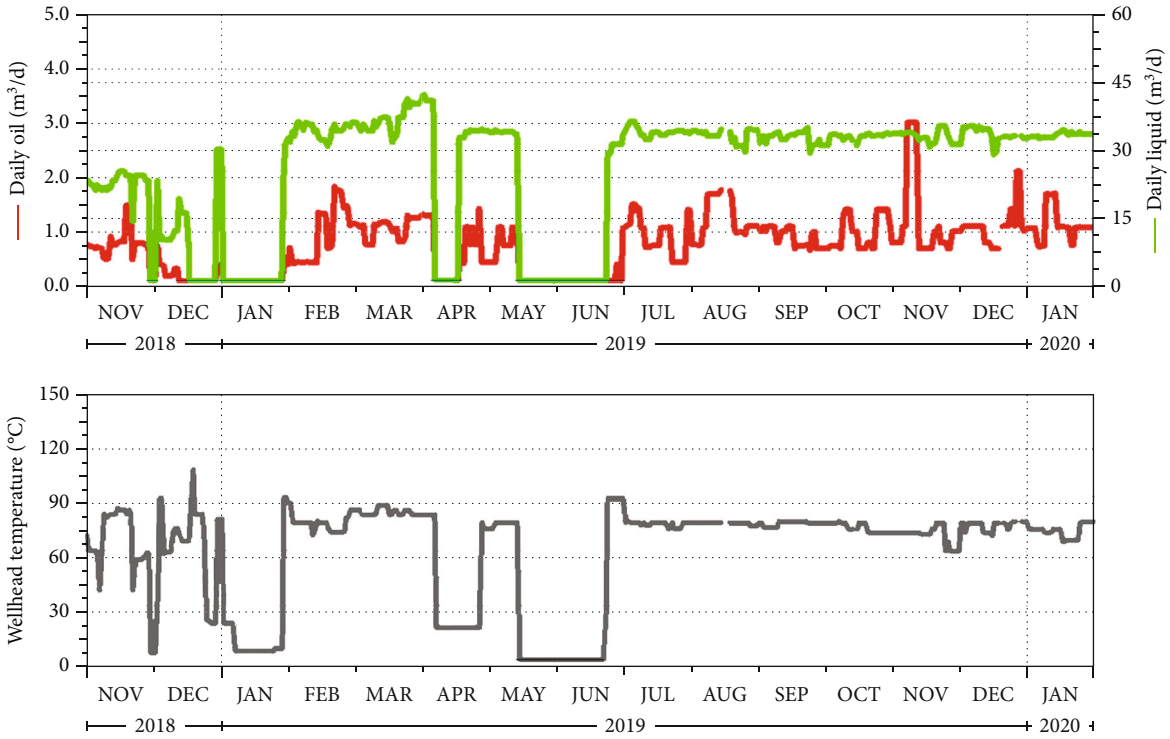

Figure 13: Typical production curves of a type II well.

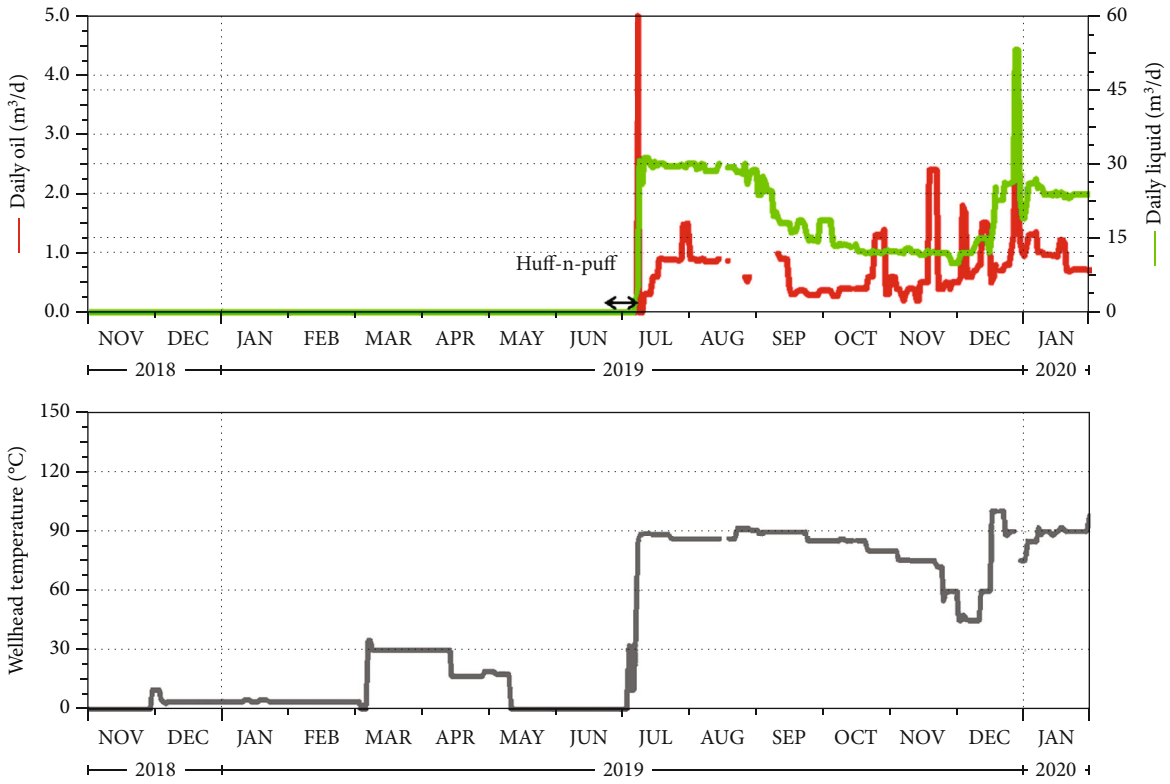

Figure 14: Typical production curves of a type III well.

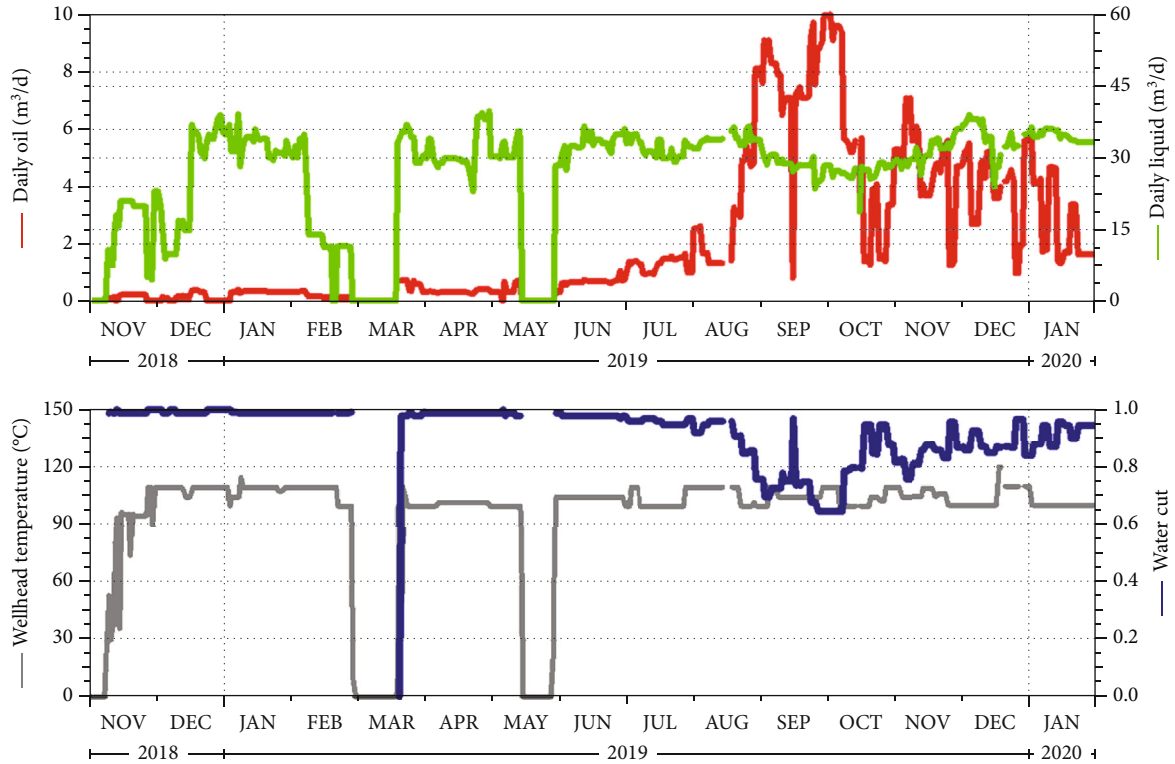

Figure 15: Typical production curves of a type IV well.

Figure 16: Emulsified foam oil produced via CO_2-steam coinjection [7, 9].

the late stage or the wells have a low fluid production volume in the long term, steam huff-n-puff can be performed to promote the connection with the steam injection well.

The type III wells were the type with low or no fluid production after conversion. Figure 14 shows the production dynamics of this type of well. These wells had poor connectivity with the steam injection wells, and during the original steam flooding, layer $J_3q_2^{2\text{-}2}$ was not effectively utilized. Usually, the liquid production volume was generally less than 8 t/d, or no liquid was produced at all. For such wells, measures such as steam huff-n-puff could be taken to accelerate the connection with the steam injection wells. The well shown in Figure 14 could not be effectively developed after conversion, and one round of steam huff-n-puff was carried out to create communication with the steam injection well.

The type IV wells exhibited a gradually increasing temperature and fluid production volume after conversion. Figure 15 shows the production dynamics of this type of well. This type of well slowly established thermal communications with the steam injection wells, leading to a gradually increasing liquid production. It can be seen from Figure 15 that this type of well exhibited a better production response

compared with the other types of wells because the oil production was more stable and the water cut was lower. Similar to the type I wells, when the liquid production volume reaches a certain threshold, the liquid production should be properly controlled to prevent steam/gas channeling.

Another interesting phenomenon was observed in the fluids produced by the CO_2-steam coinjection process. Figure 16 shows the digital images of the emulsified foam oil produced by the CO_2-steam coinjection process. This phenomenon did not occur in the steam-only-treated wells. Both the lab and field tests showed that this type of emulsified foam oil could significantly reduce the viscosity of heavy oil [16, 17]. Further research is required to reveal what mechanisms lead to the formation of this type of emulsified foam oil, which is created when steam and CO_2 are coinjected to recover heavy oil. This phenomenon mainly occurs in wells with relatively low production temperatures. It is preliminarily believed that the bottom hole oil viscosity of these wells is high, the solubility of carbon dioxide is high, and the free gas is released during the depressurization process. However, because the viscosity of the oil is high, the free gas is trapped in the oil and no continuous free gas phase is formed, so this foam oil is formed. Foam oil can help reduce the viscosity of heavy oil.

4. Conclusions

(1) By first considering the geological characteristics of the $J_3q_2^{2\text{-}1}$ and $J_3q_2^{2\text{-}2}$ layers and the remaining oil distributions in these two layers, researchers combined both into a single layer for development. The perforation intervals of the production well and the steam injection well were repositioned to the middle and lower parts of the $J_3q_2^{2\text{-}2}$ layer. The perforation thickness was decreased to 4–5 m. In the later stage of steam flooding, CO_2-assisted steam flooding was conducted. First, a large slug of steam was injected, and then, a much smaller CO_2 slug was injected.

(2) The CO_2-assisted steam flooding technique can effectively increase the formation pressure, reduce the water cut, and increase the production-injection ratio. In general, the field test showed that CO_2-assisted steam flooding effectively suppressed the steam channeling in the test area.

(3) Four types of producers, which exhibited different production responses to the CO_2-assisted steam flooding, were classified. The type IV wells responded favorably to the CO_2-assisted steam flooding treatment, while the other types of wells responded less favorably to the CO_2-assisted steam flooding treatment.

(4) The CO_2-assisted steam flooding exhibited significantly different production characteristics than those of steam flooding. One unique phenomenon observed in the fluids produced by the CO_2-assisted steam flooding process was the formation of emulsified foam oil. This emulsified foam oil could significantly reduce the viscosity of the heavy oil.

Data Availability

Data is available on request.

Disclosure

This paper is a revised version of the conference paper SPE-201832-MS presented at the SPE Russian Petroleum Technology Conference, October 2020.

Conflicts of Interest

The authors declare that they have no conflicts of interest.

Acknowledgments

We gratefully acknowledge the financial support provided by the RIPED, China National Petroleum Corporation (CNPC).

References

[1] H. Li, S. Zheng, and D. Yang, "Enhanced swelling effect and viscosity reduction of solvent(s)/co2/heavy-oil systems," *SPE Journal*, vol. 18, no. 4, pp. 695–707, 2013.

[2] L. W. Lake, *Enhanced Oil Recovery*, USA, Prentice Hall, Englewood Cliffs, 1989.

[3] A. Abedini, F. Torabi, and N. Mosavat, "Performance of immiscible and miscible CO_2 injection process in a tight carbonate reservoir (experimental and simulation approach)," *International Journal of Oil Gas Coal Technology.*, vol. 9, no. 3, pp. 265–279, 2015.

[4] Y. Zhang, Y. Wang, F. Xue et al., "CO_2 foam flooding for improved oil recovery: reservoir simulation models and influencing factors," *Journal of Petroleum Science and Engineering*, vol. 133, pp. 838–850, 2015.

[5] W. D. Peck, N. A. Azzolina, J. Ge et al., "Quantifying CO_2 storage efficiency factors in hydrocarbon reservoirs: a detailed look at CO_2 enhanced oil recovery," *International Journal of Greenhouse Gas Control*, vol. 69, pp. 41–51, 2018.

[6] Y. Hu, M. Hao, G. Chen, R. Sun, and S. Li, "Technologies and practice of CO_2 flooding and sequestration in China," *Petroleum Exploration and Development*, vol. 46, no. 4, pp. 753–766, 2019.

[7] C. Song and D. Yang, "Experimental and numerical evaluation of CO_2 huff-n-puff processes in Bakken formation," *Fuel*, vol. 190, pp. 145–162, 2017.

[8] Y. Tang, J. Tang, Q. Liu et al., "Review on phase behavior in tight porous media and microscopic flow mechanism of CO_2 huff-n-puff in tight oil reservoirs," *Geofluids*, vol. 2020, 15 pages, 2020.

[9] P. E. Baker, "An experimental study of heat flow in steam flooding," *SPE Journal*, vol. 9, no. 1, pp. 89–99, 1969.

[10] C. Wang, P. Liu, F. Wang, B. Atadurdyyev, and M. Ovluyagulyyev, "Experimental study on effects of CO_2 and improving oil recovery for CO_2 assisted SAGD in super-heavy-oil reservoirs," *Journal of Petroleum Science and Engineering*, vol. 165, pp. 1073–1080, 2018.

[11] G. G. Hoffman and I. Steinfatt, *Thermochemical Sulfate Reduction at Steam Flooding Processes-a Chemical Approach*, American Chemical Society, Washington, DC (United States), 1993.

[12] D. Weaire, S. Hutzler, S. Cox, N. Kern, M. D. Alonso, and W. Drenckhan, "The fluid dynamics of foams," *Journal of Physics: Condensed Matter*, vol. 15, no. 1, pp. S65–S73, 2003.

[13] D. W. Zhao, J. Wang, and I. D. Gates, "Optimized solvent-aided steam-flooding strategy for recovery of thin heavy oil reservoirs," *Fuel*, vol. 112, pp. 50–59, 2013.

[14] X. Li, "Experimental study on the effect of temperature and injection pressure on CO_2 flooding," *Petroleum Geology and Recovery Efficiency.*, vol. 22, no. 1, pp. 84–87, 2015.

[15] S. U. N. Xinge, M. A. Hong, and Z. H. A. O. Changhong, "Research on ultraheavy oil development by steam stimulation converting into steamdrive combination process in Fengcheng oil field," *Xinjiang Petroleum Geology*, vol. 36, no. 1, pp. 61–64, 2015.

[16] C. Xi, Z. Qi, Y. Zhang et al., "CO_2 assisted steam flooding in late steam flooding in heavy oil reservoirs," *Petroleum Exploration and Development*, vol. 46, no. 6, pp. 1242–1250, 2019.

[17] C. Xi, Z. Qi, T. Liu et al., "CO_2 assisted steam flooding technology after steam flooding - a case study in block J6 of Xinjiang oilfield. SPE 196767," 2019.